Properties of Fr-like Th^{3+} from rf spectroscopy of high-L Th^{2+} Rydberg ions

Julie A. Keele, Chris S. Smith, and S. R. Lundeen

Department of Physics, Colorado State University, Fort Collins, Colorado 80523, USA

C. W. Fehrenbach

J. R. Macdonald Laboratory, Kansas State University, Manhattan, Kansas 66506, USA

Relative positions of twenty $n = 28$ Rydberg levels of Th^{2+} with $L = 9$, 10, 11, and 12 were determined with sub-MHz precision using the rf-RESIS (resonant excitation Stark ionization spectroscopy) technique. The pattern of binding energies was analyzed with the effective potential model, modified to account for significant nonadiabatic effects. The analysis yielded measurements of several properties of the Fr-like Th^{3+} core ion, including the quadrupole moment, $Q = 0.5931(14)$ a.u.; hexadecapole moment, $\Pi = -0.69(28)$ a.u.; g factor, $g_J = 1.24(48)$; scalar and tensor dipole polarizabilities, $\alpha_{D,0} = 15.224(33)$ a.u. and $\alpha_{D,2} = -5.30(11)$ a.u.; scalar quadrupole polarizability, $\alpha_{Q,0} = 60(15)$ a.u.; and the reduced dipole and octupole matrix elements connecting the ground $5f\ ^2F_{5/2}$ level with the low-lying $6d\ ^2D_{3/2}$ level, $|\langle ^2F_{5/2}||\mathrm{M}^{[1]}||^2D_{3/2}\rangle| = 1.436(2)$ a.u. and $|\langle ^2F_{5/2}||\mathrm{M}^{[3]}||^2D_{3/2}\rangle| = 3.3(1.1)$ a.u. The measured properties are compared with theoretical predictions.

PACS number(s): 32.30.Bv, 32.10.Dk, 32.10.Fn

I. INTRODUCTION

The pattern of binding energies of a nonpenetrating high-L Rydberg electron can serve as a sensitive probe of many properties of the positive ion binding it in its orbit. Properties such as permanent moments and polarizabilities lift the hydrogenic degeneracy that would prevail if only the core ion's total charge were significant, and produce characteristic patterns whose shape and size can be related to the underlying properties. The formal connection between these fine-structure patterns and the underlying core properties relies on a perturbative description of a Rydberg system that differs only slightly from the zeroth-order picture of a hydrogenic electron bound to a free core ion [1]. The Rydberg eigenstates are characterized by their principal quantum number n, their angular momentum L, and by their total angular momentum exclusive of Rydberg spin K, where

$$\vec{K} = \vec{L} + \vec{J}_c, \qquad (1)$$

and J_c is the angular momentum of the core ion in its ground state. In the case studied here, Rydberg levels of the Th^{2+} ion, the core ion is Fr-like Th^{3+}. This ion has a single valence electron outside of a Rn-like $(6p)^6$ core, but because of the high nuclear charge the lowest valence level is not a $7s\ ^2S_{1/2}$ level, but is instead a $5f\ ^2F_{5/2}$ level. Consequently, the pattern of Rydberg binding energies to this ion is very complex, with six eigenstates for each value of L, and K ranging from $L - 5/2$ to $L + 5/2$.

An initial study of high-L Rydberg levels of Th^{2+} was reported in 2011, using the resonant excitation Stark ionization spectroscopy (RESIS) method [2]. Three different Rydberg excitation spectra, $n = 27 - 60$, 28–66, and 29–72, were observed with partially resolved structure due to the binding energy patterns of interest. It was apparent from the observed spectra that the fine-structure patterns were significantly altered by nonadiabatic effects due to the low-lying $6d$ levels. Fortunately, the positions of these two core levels were known [3,4], and this made it possible to treat the portion of the perturbation energies due to intermediate

levels containing these two core levels separately, with the remainder of the structure accounted for by a modified effective potential. Using this model, fourteen well resolved excitation lines were identified, and their positions were fit to extract measurements of the quadrupole moment, the scalar and tensor dipole polarizabilities, and the reduced dipole matrix elements coupling the ground state to the two $6d$ levels. The scope of these conclusions was limited by the lack of full resolution of the fine-structure patterns and their precision was limited by the ± 20 MHz precision of the optical spectra. The study reported here uses the rf-RESIS double resonance method to directly measure fine-structure intervals within the $n = 28$ level of Th^{2+}, detecting the transitions by their effect on the population of a single fine-structure level, as reflected in the $n = 28$–66 RESIS excitation spectra. The relative positions of twenty $n = 28$ levels with $L = 9$, 10, 11, and 12 were determined experimentally with precision of better than ± 0.5 MHz. Analysis of this more complete and more precise data pattern gives much better information about the properties of the Th^{3+} core.

Measurements of Th^{3+} properties are interesting for a number of reasons. Due to its high nuclear charge and large number of electrons, its theoretical description is very challenging even for the most advanced atomic structure methods. Even the identification of its ground state differs among several common theoretical approaches. Fortunately, there is a small amount of spectroscopic data [3] that established that the $^2F_{5/2}$ level is the true ground state. Those measurements also establish that the $5f$, $6d$, and $7s$ valence levels are in close proximity in Th^{3+}, adding to the difficulty of the theoretical calculations [5]. Measurements of properties such as permanent moments and polarizabilities, which are much more sensitive to errors in the wave function than term energies, can test the accuracy of alternative theoretical approaches. Since the Th^{3+} ion is one of the possible ionization states of Th in chemical compounds [6], these tests can help to improve confidence in *a priori* descriptions of thorium chemistry. The isolated Th^{3+} ion also currently figures in an effort to build an ultrahigh-precision clock based on a narrow nuclear transition in ^{229}Th. One
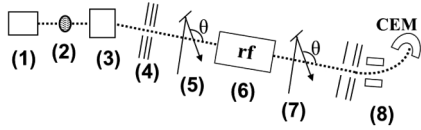
FIG. 1. Diagram of the rf-RESIS apparatus. A beam of the ion of interest, Th^{3+}, is produced with an ECR and selected for its mass and charge at (1). The beam then charge captures an electron from a dense $10F$ Rb Rydberg target at (2), thus becoming a beam of highly excited Th^{2+} Rydberg states. The remaining Th^{3+} beam is removed from the apparatus at (3) by the charge selection of the Th^{2+} Rydberg beam. An einzel lens then focuses the beam and ionizes weakly bound Rydberg states at (4). The Rydberg beam then intersects a Doppler-tuned CO_2 laser in the first laser interaction region at (5), exciting population from one specific $n = 28$ (L,K) level to the $n = 66$ level. This excitation depletes the population of the $n = 28$ (L,K) level. The population of the $n = 28$ (L,K) level is then replenished by an rf transition with another state in the $n = 28$ levels when the beam passes through the rf region at (6). The second laser interaction region at (7) then excites the population of the $n = 28$ (L,K) level again. At (8) the population of the $n = 66$ level is then Stark ionized and deflected into a CEM. The electric field in the rf region is modulated, and the synchronous change in the Th^{3+} current is measured as a function of the frequency of the electric field in the rf region.

approach is to trap and cool the $^{229}Th^{3+}$ ion and drive the nuclear transition through a sequence of stepwise laser transitions in the Th^{3+} ion, one of which will connect the two nuclear levels [4,7]. Progress towards this goal relies in part on theoretical calculations of level positions and transition probabilities in the Th^{3+} ion.

Section II of this paper describes the measurements. The resulting map of the relative positions of twenty $n = 28$ fine-structure levels is a purely experimental result, independent of any particular theoretical model of the fine-structure patterns. Section III describes the model used here to interpret the measurements and the fit that was used to extract core properties from the data pattern. Section IV compares the measured properties with previous measurements and with theoretical calculations.

II. EXPERIMENT

The measurements reported here were obtained with the same Rydberg beam apparatus used for the optical RESIS study [2], Fig. 1. A beam of 75-keV Th^{3+} ions was extracted from an electron cyclotron resonance (ECR) ion source, and sent through a Rb $10F$ Rydberg target where a small fraction of the beam captured a single electron to form a beam of highly excited Th^{2+} Rydberg ions. A magnet selected the Th^{2+} beam, and an einzel lens focused the beam and ionized very weakly bound Rydberg ions. For this experiment, the Rydberg beam encountered two regions where it interacted with a Doppler-tuned CO_2 laser, and between these two regions it passed through a region where a radio-frequency (rf) electric field was applied. Both laser interaction regions (LIRs) are tuned to the same RESIS excitation transition in the $n = 28$–66 spectrum, and the rf region drives a transition directly between two different fine-structure levels within the $n = 28$ manifold, one of which is being excited in the two laser regions. This combination of interactions results in additional excitation

when the rf region is on resonance, providing detection of the rf resonance. After the second LIR, the Rydberg ions enter a region of strong electric field that Stark ionizes any ions that have been excited to $n = 66$ and deflects the resulting Th^{3+} ions into a channel electron multiplier (CEM). The component of the CEM current that is synchronous with chopping of the rf electric field is measured as a function of the rf frequency to reveal the resonance. The noise in the measured rf signal is dominated by shot noise in the background count rate, and is conveniently estimated by noting the noise in the output of the lock-in amplifier that is $90°$ out of phase with the modulation of the rf electric field.

The rf interaction region used in this study is described in detail elsewhere [8]. It is an eccentric coaxial transmission line in which the rf electric field propagates either parallel or antiparallel to the Rydberg beam. Each measured resonance was observed in both directions of propagation, and the line centers averaged to remove Doppler shifts. As a check on possible stray electric fields within the rf region, which could Stark shift the resonances studied here, the $n = 37$, $L = 12$–15 transition in Th^{3+} Rydberg levels was observed frequently during the course of this study. The position of this resonance at zero stray electric field was determined in a recent study [9], and its consistent agreement with that position indicated that average stray electric field was less than 0.001 $(V/cm)^2$ and thus not a significant factor in the present study.

The most significant challenge in this study was finding a way to measure enough rf transitions to define the relative positions of a sufficient number of levels within the $n = 28$ manifold to improve the measurements of Th^{3+} properties already reported. This was made difficult by the lack of complete resolution of the optical RESIS spectrum. For example, in the $n = 28$–66 spectrum reported in Ref. [2], only three levels within $n = 28$, one each with $L = 8$, 9, and 10, were among the 14 levels identified as isolated excitations and used in fitting for the core properties. Fortunately, once an estimate of core properties was obtained through that fit, simulations based on those properties reproduced virtually all of the features of the three observed spectra, and made it possible to identify many more lines in the $n = 28$–66 spectrum [2,10]. Figure 2, for example, shows a section of the $n = 28$–66 spectrum with many different lines identified. They are labeled there by the values of L and K in the $n = 28$ level being excited. Notice that five of the six $L = 9$ levels contribute to four well isolated peaks in the spectrum. This provided a starting point for the rf study, along with the estimates of the $n = 28$ fine-structure intervals derived from the same core properties.

The strongest rf transitions satisfy $\Delta L = \Delta K$, i.e., they connect levels belonging to the same "series" and having $K = L + \kappa$, with κ a constant. The five $L = 9$ levels identified in Fig. 2 provide access to the five series with $-\frac{5}{2} \leqslant \kappa \leqslant \frac{3}{2}$. As a first step in the rf study, the relative positions of the four members of each of these series with $L = 9$, 10, 11, and 12 were determined. Figure 3 shows an example of this process for the $\kappa = 3/2$ series. In this case, both LIRs were tuned initially to excite the $(L,K) = (9,10.5)$ level. The rf frequency was then varied until the transition to the $(10,11.5)$ level was discovered near 1503 MHz. An example of such an observation is shown in Fig. 3. Retuning LIR2 to the unresolved position in the optical spectrum where the $(10,11.5)$ level is excited
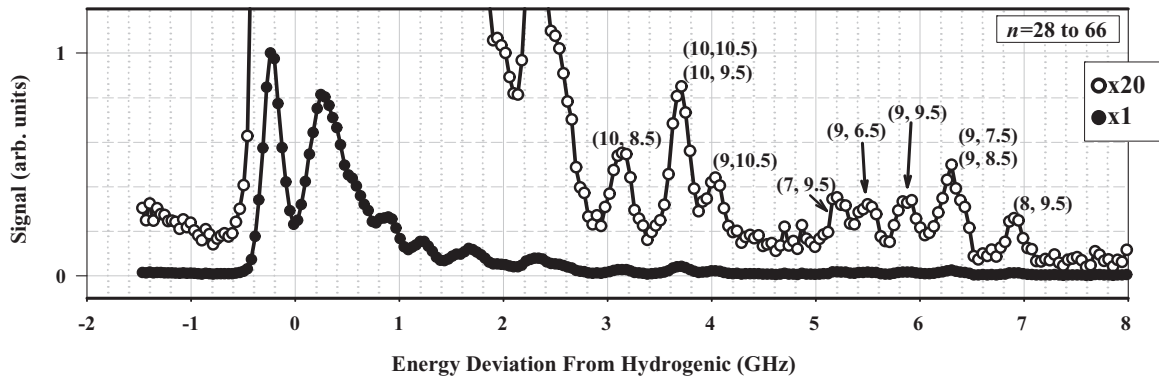
FIG. 2. RESIS optical excitation spectrum for the $n = 28$–66 transition. The x axis is the deviation from the hydrogenic transition frequency in GHz. The original signal is indicated by the solid black points while the signal times 20 is shown by the open circles. Each of the resolved structures has been identified by its (L,K) values in the lower-n state of the RESIS excitation transition, $n = 28$. The identifications were completed using the result from the optical RESIS study [2].

recovered the rf signal with negative sign, corresponding to a decrease in excitation of the (10,11.5) level when the rf is on resonance. Then moving LIR1 by the same angle resulted in both LIRs being tuned to excite the (10,11.5) level, and made it possible to discover the transition from (10,11.5) to (11,12.5) near 885 MHz. An example of this resonance is also shown in Fig. 3. Finally, leaving both LIRs tuned on the (10,11.5) excitation, a two-photon transition between the (10,11.5) and the (12,13.5) levels was discovered near 718 MHz, corresponding to an energy separation of about

1436 MHz. An example of this resonance is also shown in Fig. 3, plotted vs twice the applied frequency. By this combination of three observations, the relative position of all four of these levels was determined very precisely, even though only one of them was well resolved in the optical RESIS spectrum.

A similar process was carried out for the other four series represented by the $L = 9$ levels identified in Fig. 2. Finally, four weaker transitions, with $\Delta K = 0$, were observed to determine the relative positions of the different series. The
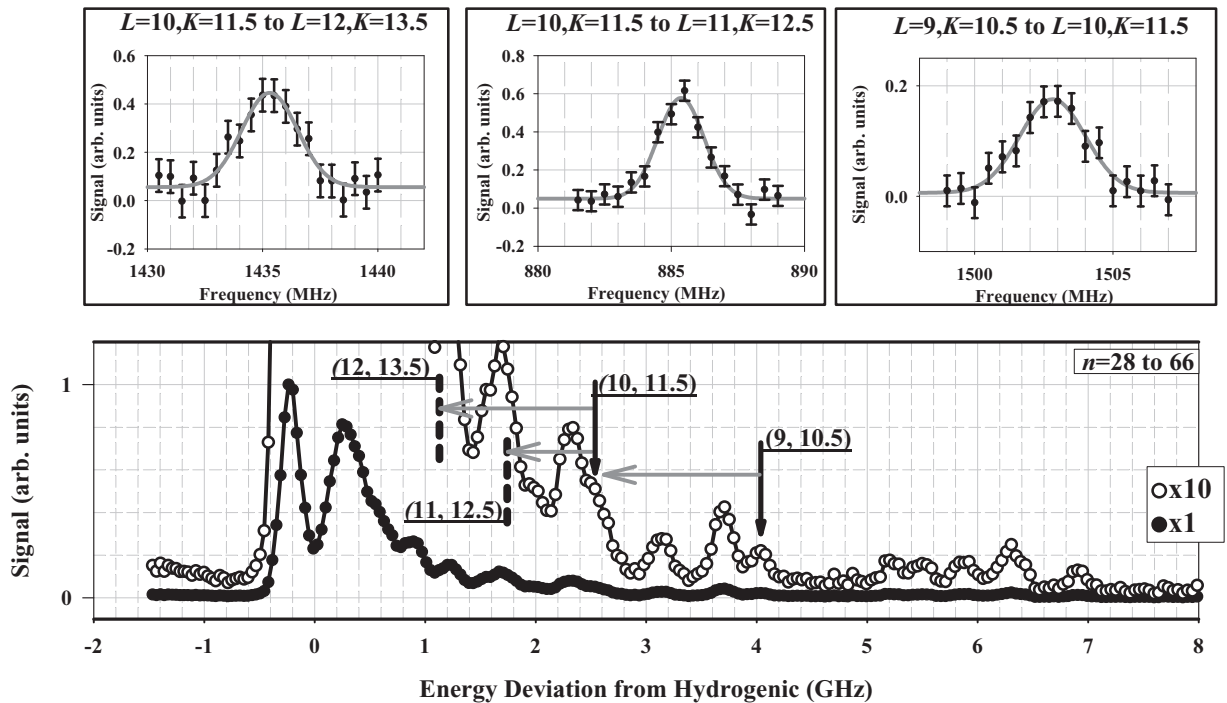

FIG. 3. Illustration of the procedure used to measure the relative positions of the L–3/2 series in the $n = 28$ Th²⁺ Rydberg fine structure. The bottom graph is the optical excitation spectrum for the $n = 28$–66 transition, the location of each of the transitions involved in the L–3/2 series is denoted by a vertical line. The solid vertical lines denote resolved transitions that were used in the detection of rf transitions. The dashed vertical lines were transitions whose positions were determined from rf transitions. The horizontal lines interconnecting the levels indicate rf transitions observed. Examples of the each of the three rf transitions used to map out the levels in the L–3/2 series are also shown. Each of the rf resonances was fit to determine the frequency difference between states to sub-MHz precision.

TABLE I. Summary of measured rf intervals between $n = 28$ levels of Th^{2+}. The intervals are identified in columns 1 and 2 by the value of κ, and by the (L,K) values for the two levels. Column 3 gives the final measured result of the interval, in MHz. The statistical uncertainty is shown in parentheses. Column 4 indicates the number of independent observations of the interval that were made. Column 5 shows the initial estimate of the interval derived from the core properties reported in Ref. [2], which guided the search for the resonances.

$\kappa = K{-}L$	Transition	Measured (MHz)	No. Obs.	Estimate (MHz)
−2.5	(9,6.5)–(10,7.5)	3492.42(11)	3	3486(35)
−2.5	(10,7.5)–(11,8.5)	1763.64(8)	4	1775(27)
−2.5	(10,7.5)–(12,9.5)	2168.86(7)	4	2192(54)
−1.5	(9,7.5)–(10,8.5)	3126.56(11)	4	3117(30)
−1.5	(10,8.5)–(11,9.5)	1663.47(8)	4	1669(16)
−1.5	(10,8.5)–(12,10.5)	2262.15(11)	4	2273(22)
−0.5	(9,8.5)–(10,9.5)	2683.02(16)	4	2689(79)
−0.5	(10,9.5)–(11,10.5)	1504.90(11)	4	1511(47)
−0.5	(10,9.5)–(12,11.5)	2221.73(12)	4	2230(75)
0.5	(9,9.5)–(10,10.5)	2257.30(25)	2	2166(93)
0.5	(10,10.5)–(11,11.5)	1270.18(13)	4	1264(56)
0.5	(10,10.5)–(12,12.5)	1989.52(5)	4	1981(91)
1.5	(9,10.5)–(10,11.5)	1501.69(7)	4	1505(59)
1.5	(10,11.5)–(11,12.5)	884.60(6)	4	884(34)
1.5	(10,11.5)–(12,13.5)	1433.91(10)	4	1431(56)
1.5 to 0.5	(9,10.5)–(10,10.5)	388.52(11)	5	423(23)
0.5 to − 0.5	(10,10.5)–(11,10.5)	1427.10(10)	5	1400(81)
−0.5 to − 1.5	(10,9.5)–(11,9.5)	2328.73(19)	4	2288(138)
−1.5 to − 2.5	(10,8.5)–(11,8.5)	2982.60(12)	4	2909(155)

final result was determination of 19 energy intervals that determined the relative positions of 20 of the 24 levels with

TABLE II. Relative energies, in MHz, of the $n = 28$ Rydberg levels of Th^{2+} with $9 \leqslant L \leqslant 12$. Column 1 identifies the level by its quantum numbers (L,K). One level, (12,9.5), has been arbitrarily taken to have zero energy, and the energies of all the other levels were computed from the intervals reported in Table I. One series of levels, with $K = L + 2.5$, was not located.

(L,K)	E (MHz)
(9,6.5)	−5661.28(13)
(9,7.5)	−6514.38(16)
(9,8.5)	−6736.10(31)
(9,9.5)	−6232.58(39)
(9,10.5)	−4363.80(32)
(9,11.5)	—
(10,7.5)	−2168.86(7)
(10,8.5)	−3387.82(16)
(10,9.5)	−4053.08(26)
(10,10.5)	−3975.28(30)
(10,11.5)	−2862.11(33)
(10,12.5)	—
(11,8.5)	−405.22(11)
(11,9.5)	−1724.35(18)
(11,10.5)	−2548.18(28)
(11,11.5)	−2705.10(33)
(11,12.5)	−1977.51(33)
(11,13.5)	—
(12,9.5)	0.00
(12,10.5)	−1125.67(19)
(12,11.5)	−1831.35(29)
(12,12.5)	−1985.76(30)
(12,13.5)	−1428.20(34)
(12,14.5)	—

$L = 9$, 10, 11, and 12 within the $n = 28$ manifold of Th^{2+}. Table I summarizes the measured intervals. Column 1 gives the κ value for the transition, and column 2 identifies the transition by the (L,K) values for both levels involved. Column 3 gives the final measured value of the interval, with the statistical uncertainty in parentheses. Column 4 reports the number of independent measurements of the interval. Column 5 shows the interval estimate made from the core parameters determined from the optical RESIS study [2]. These determined the search range for the rf resonances. For the five two-photon transitions, a small ac shift correction, which ranged from 0.10 to 0.17 MHz, was calculated and applied. The ac shift rates calculated in a similar manner were tested by measurement in a recent study [9] and found to be accurate to 20%. The small size of the shift rates calculated here makes a 20% uncertainty negligible compared to other uncertainties.

The relative positions of the 20 levels connected by the measured intervals are shown in Table II. One level, the $(L,K) = (12,9.5)$ has been arbitrarily taken to have zero energy since only the relative positions are determined by the measurements. The uncertainties in the positions are found from propagation of the interval measurement errors, and in all cases are less than 0.5 MHz. One series, with $\kappa = 2.5$, is not included since none of its members was resolved in the optical RESIS spectrum. Figure 4 illustrates the pattern of energy levels determined by these measurements.

III. ANALYSIS

The measured pattern of binding energies contains a great deal of information about the properties of the Th^{3+} core. In many respects, this pattern is analogous to the pattern of $n = 9$ binding energies recently studied in the nickel atom [8]. In both cases, the core ion has $J_c = 5/2$, leading to patterns

of similar complexity. In the nickel case, the analysis was relatively simple. Except for some small corrections, discussed below, the measured energy level pattern is expected to be given by the expectation value of the effective potential, a sum of terms proportional to scalar products of tensor operators of rank 0–4. The coefficient of each term is given by a series of hydrogenic radial expectation values, rapidly convergent for high-L levels, multiplied by specific core properties [1].

$$V_{\text{eff}} = -\left[\frac{\alpha_{D,0}}{2r^4} + \frac{(\alpha_{Q,0} - 6\beta_{D,0})}{2r^6} + \cdots\right] + \left[-\frac{\alpha_{FS}^2 g_J}{2r^3} + \frac{\beta_{D,1}}{r^6} + \cdots\right]\vec{L}\cdot\vec{J}_c - \left[\frac{Q}{r^3} + \frac{\alpha_{D,2}}{2r^4} + \cdots\right]\frac{X^{[2]}(J_c)\cdot C^{[2]}(\hat{r})}{\begin{pmatrix} J_c & 2 & J_c \\ -J_c & 0 & J_c \end{pmatrix}}$$
$$+\left[-\frac{C_{M3}}{r^5} + \frac{(\beta_{Q,3} + \beta_{DO,3})}{r^8} + \cdots\right]X^{[3]}(J_c)\cdot T^{[3]}(\hat{r}) - \left[\frac{\Pi}{r^5} + \frac{(\alpha_{Q,,4} + \alpha_{DO,4})}{2r^6} + \cdots\right]\frac{X^{[4]}(J_c)\cdot C^{[4]}(\hat{r})}{\begin{pmatrix} J_c & 4 & J_c \\ -J_c & 0 & J_c \end{pmatrix}}. \quad (2)$$

Equation (2) shows the first two terms for each tensor order. Normally the second term is a small correction to the first. The study of $n = 9$ nickel Rydberg levels confirmed this pattern [8].

Unfortunately, the Th²⁺ Rydberg structure cannot be analyzed so simply. Most of the terms in the effective potential are derived from the second-order perturbation energies, using the "adiabatic expansion" of the energy denominators that

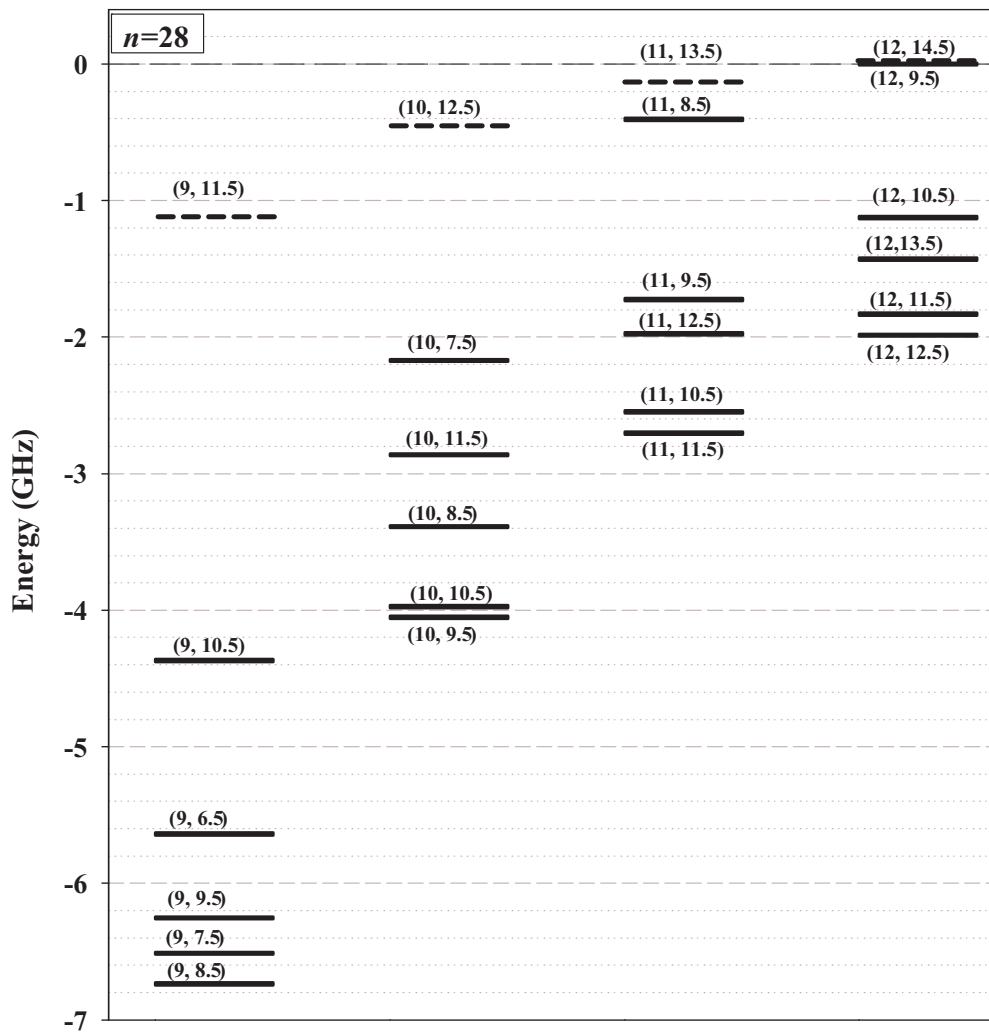FIG. 4. The fine structure of the $n = 28$ Th²⁺ Rydberg levels; each level is labeled by (L,K). The levels denoted with solid lines were levels measured using rf transitions. Levels denoted with dashed lines are levels that were not measured during the rf study; the positions of those levels have been inferred from the result of the rf study. The position of the (12,9.5) level was arbitrarily taken to be zero.

occur and manipulating the resulting expressions by taking advantage of the properties of the zeroth-order hydrogenic Rydberg wave functions. This works well if all of the excited states of the core ion are high enough in energy that the core ion responds approximately adiabatically to the motion of the Rydberg electron. In the case of Th^{3+}, the two $6d$ levels are close enough to the ground state that they fail this test, and their contributions to the second-order perturbation energies are said to be nonadiabatic. Consequently, these contributions do not scale as predicted by Eq. (2). One way to account for this is to segregate the contributions of intermediate levels containing these two $6d$ core levels from the rest of the second-order perturbation energy. These $6d$ contributions can be calculated up to a constant that is equal to the square of the reduced dipole matrix element coupling each level to the Th^{3+} ground state. For example, the lowest multipole contribution to the second-order energy due to intermediate states containing the $6d$ $^2D_{3/2}$ core level is given by

$$
\begin{aligned}
E_{DD}^{[2]}(^2D_{3/2}) = -\langle^2F_{5/2}||M^{[1]}||^2D_{3/2}\rangle^2 \sum_{n'L'} \left\{ \begin{matrix} K & L & \frac{5}{2} \\ 1 & \frac{3}{2} & L' \end{matrix} \right\}^2 \\
\times \begin{pmatrix} L & 1 & L' \\ 0 & 0 & 0 \end{pmatrix}^2 (2L+1)(2L'+1) \\
\times \frac{[nL|r^{-2}|n'L']^2}{\Delta E(^2D_{3/2}) + E(n') - E(n)},
\end{aligned}
\tag{3}
$$

where $[nL|r^{-2}|n'L']$ is a hydrogenic radial integral. If the core excitation energy is known, which it is in this case, the sum over n' can be evaluated without approximation, and the entire result is known except for the value of the squared reduced dipole matrix element that occurs first. The remainder of the second-order energy contributes to a modified effective potential that contains the contributions of all other core excited states. With this approach, it is expected that

$$
\begin{aligned}
E_{\text{corr}} = \langle V_{\text{eff}}^{\text{Mod}} \rangle + \langle^2F_{5/2}||M^{[1]}||^2D_{3/2}\rangle^2 E_{DD}^{[2]}(^2D_{3/2})^* \\
+ \langle^2F_{5/2}||M^{[1]}||^2D_{5/2}\rangle^2 E_{DD}^{[2]}(^2D_{5/2})^*,
\end{aligned}
\tag{4}
$$

where $E_{DD}^{[2]}(^2D_{3/2})^*$ represents the second-order perturbation energy due to intermediate states containing the $6d$ $^2D_{3/2}$ core state, calculated at unit value of the dipole coupling matrix element, and similarly for the $^2D_{5/2}$ level. The modified effective potential, $V_{\text{eff}}^{\text{Mod}}$, describes the effect of all excited states other than the $6d$ levels. This was the approach used to fit the optical RESIS data [2], and in that case $V_{\text{eff}}^{\text{Mod}}$ was truncated to include only the three most significant core properties, $\alpha_{D,0}$, $\alpha_{D,2}$, and Q. Those fits confirmed that the effects of the $6d$ levels were very large, contributing more than 5000 MHz to the binding energies of some of the levels.

Certainly, something similar will be required to analyze the rf data. The nonadiabatic effects of the $6d$ levels must be included in the analysis. In view of the high precision of the experimental measurements, and the large size of the dipole-dipole second-order energies involving the $6d$ levels, other contributions from the $6d$ levels were also explored. Two other

TABLE III. Calculated values of the second-order perturbation energies arising from intermediate levels containing $6d$ core levels. Column 1 shows the (L,K) values for the $n = 28$ Rydberg levels of Th^{2+} studied here. Columns 2 and 3 show the calculated dipole-dipole energy contribution from $^2D_{3/2}$ and $^2D_{5/2}$ core levels. Columns 4 and 5 show the calculated octupole-dipole energy contributions from $^2D_{3/2}$ and $^2D_{5/2}$ core levels. All results are in MHz. The coupling matrix elements assumed for these calculations are $\langle 5f\,^2F_{5/2}||M^{[1]}||6d\,^2D_{3/2}\rangle = -1.530$ a.u. $\langle 5f\,^2F_{5/2}||M^{[1]}||6d\,^2D_{5/2}\rangle = 0.412$ a.u. $\langle 5f\,^2F_{5/2}||M^{[3]}||6d\,^2D_{3/2}\rangle = 8.394$ a.u. $\langle 5f\,^2F_{5/2}||M^{[3]}||6d\,^2D_{5/2}\rangle = -7.043$ a.u.

(L,K)	$E_{DD}^{[2]}(^2D_{3/2})$	$E_{DD}^{[2]}(^2D_{5/2})$	$E_{OD}^{[2]}(^2D_{3/2})$	$E_{OD}^{[2]}(^2D_{5/2})$
(9,6.5)	−7420.58	−37.48	−69.43	−3.41
(9,7.5)	−4947.05	−83.17	69.43	−1.59
(9,8.5)	−2820.68	−113.20	23.77	3.53
(9,9.5)	−1295.33	−119.40	−32.74	4.14
(9,10.5)	−654.73	−92.66	10.52	−2.13
(9,11.5)	−1212.46	−22.91	−5.98	−1.10
(10,7.5)	−3458.32	−18.82	−22.13	−1.08
(10,8.5)	−2282.49	−43.80	23.01	−0.59
(10,9.5)	−1310.04	−59.99	6.68	1.15
(10,10.5)	−654.86	−63.49	−10.73	1.43
(10,11.5)	−442.85	−49.98	4.71	−0.59
(10,12.5)	−811.90	−14.73	−2.73	−0.48
(11,8.5)	−1342.74	−10.89	−5.42	−0.41
(11,9.5)	−878.89	−26.17	5.82	−0.25
(11,10.5)	−519.89	−35.93	1.13	0.46
(11,11.5)	−311.85	−38.04	−2.70	0.58
(11,12.5)	−305.27	−30.15	2.23	−0.20
(11,13.5)	−555.04	−9.72	−1.31	−0.22
(12,9.5)	−748.71	−6.78	−2.05	−0.18
(12,10.5)	−486.66	−16.69	2.26	−0.11
(12,11.5)	−292.89	−22.93	0.30	0.20
(12,12.5)	−192.83	−24.26	−1.03	0.26
(12,13.5)	−214.12	−19.30	1.10	−0.08
(12,14.5)	−386.61	−6.58	−0.66	−0.11

multipole contributions to the second-order energy involving these core levels are the octupole-dipole and octupole-octupole terms. Both would be expected to be highly nonadiabatic. Estimates based on calculated dipole [11] and octupole matrix elements [12] indicate that the octupole-octupole terms are negligible but the octupole-dipole terms could be quite significant. Table III shows, for all the levels of this study, calculated values of the dipole-dipole and octupole-dipole second-order energies involving $6d$ core levels, assuming calculated values of the coupling matrix elements. Since, in both cases, the contribution from the $^2D_{5/2}$ core state is much smaller than the contribution from the $^2D_{3/2}$ state, and since the ratios of the reduced matrix elements to the two $6d$ levels are expected to be close to the ratio predicted by LS coupling, the total contribution of the two $6d$ levels can be parametrized by the two matrix elements, dipole and octupole, that connect the $^2F_{5/2}$ ground state and the $6d$ $^2D_{3/2}$ level. The remainder of the energies should be accounted for by the modified effective

TABLE IV. Corrections applied to the measured positions prior to fitting to extract core properties. The first column lists the (L,K) values for the $n = 28$ Rydberg levels of Th^{2+} studied here. The second column gives the relativistic correction for each of the levels. The third column gives the correction necessary for the coupling of the studied Rydberg states with other Rydberg states. The fourth column gives the correction necessary for the coupling of the studied Rydberg states with other Rydberg states in $n = 28$. The fifth column gives the corrections for the assumption of the zeroth-order energy in the second-order dipole-dipole energies for the low-lying $6d$ states. The final column is the total of all the corrections. All results are in MHz.

(L,K)	E_{Rel}	$E^{[2]}$ (V_{eff})	E ($\alpha_{D,2}$ shift)	$E^{[2]}_{\text{correction}}(^2D_{3/2})$	$E_{\text{Corrections}}$
(9,6.5)	−50.73	−0.82(3.90)	3.10(0.03)	65.09(7.22)	16.64(8.21)
(9,7.5)	−50.73	−1.72(2.92)	7.94(0.08)	−20.23(5.14)	−64.75(5.92)
(9,8.5)	−50.73	−3.20(3.22)	13.93(0.20)	−17.55(2.82)	−57.54(4.28)
(9,9.5)	−50.73	−4.59(3.50)	−132.78(20.58)	6.53(0.98)	−181.58(20.90)
(9,10.5)	−50.73	−5.06(3.08)	−3.12(0.02)	0.00(0.00)	−58.91(3.08)
(9,11.5)	−50.73	−3.81(3.47)	2.57(0.16)	0.00(0.00)	−51.97(3.48)
(10,7.5)	−44.25	0.26(0.79)	0.94(0.01)	10.24(0.96)	−32.81(1.24)
(10,8.5)	−44.25	0.60(0.53)	2.82(0.04)	−3.64(0.64)	−44.48(0.83)
(10,9.5)	−44.25	0.30(0.62)	6.72(0.20)	−2.98(0.35)	−40.20(0.74)
(10,10.5)	−44.25	−0.32(0.69)	−11.87(0.76)	1.01(0.12)	−55.43(1.04)
(10,11.5)	−44.25	−0.92(0.57)	−1.95(0.02)	0.00(0.00)	−47.11(0.57)
(10,12.5)	−44.25	−1.33(0.69)	0.92(0.06)	0.00(0.00)	−44.66(0.69)
(11,8.5)	−38.90	0.17(0.06)	0.33(0.00)	0.14(0.01)	−38.25(0.06)
(11,9.5)	−38.90	0.40(0.03)	1.04(0.00)	−0.05(0.01)	−37.51(0.03)
(11,10.5)	−38.90	0.20(0.04)	3.00(0.02)	−0.04(0.01)	−35.73(0.05)
(11,11.5)	−38.90	−0.19(0.05)	−2.93(0.18)	0.02(0.01)	−42.00(0.19)
(11,12.5)	−38.90	−0.55(0.04)	−1.33(0.19)	0.00(0.00)	−40.78(0.19)
(11,13.5)	−38.90	−0.82(0.05)	0.40(0.03)	0.00(0.00)	−39.31(0.06)
(12,9.5)	−34.40	0.14(0.01)	0.19(0.00)	0.00(0.00)	−34.07(0.01)
(12,10.5)	−34.40	0.38(0.00)	0.59(0.00)	0.00(0.00)	−33.43(0.00)
(12,11.5)	−34.40	0.27(0.00)	1.87(0.02)	0.00(0.00)	−32.26(0.02)
(12,12.5)	−34.40	−0.02(0.01)	−1.14(0.08)	0.00(0.00)	−35.56(0.08)
(12,13.5)	−34.40	−0.30(0.00)	−0.98(0.22)	0.00(0.00)	−35.67(0.22)
(12,14.5)	−34.40	−0.46(0.01)	0.19(0.02)	0.00(0.00)	−34.66(0.02)

potential.

$$
\begin{aligned}
E_{\text{corr}} = {} & \left\langle V_{\text{eff}}^{\text{Mod}} \right\rangle + \langle ^2F_{5/2}||M^{[1]}||^2D_{3/2}\rangle^2 \\
& \times \left[E^{[2]}_{DD}(^2D_{3/2})^* + \frac{1}{14}E^{[2]}_{DD}(^2D_{5/2})^* \right] \\
& + \langle ^2F_{5/2}||M^{[1]}||^2D_{3/2}\rangle \langle ^2F_{5/2}||M^{[3]}||^2D_{3/2}\rangle \\
& \times \left[E^{[2]}_{DO}(^2D_{3/2})^* + \frac{1}{\sqrt{21}}E^{[2]}_{DO}(^2D_{5/2})^* \right]. \quad (5)
\end{aligned}
$$

Each of the second-order energies in Eq. (5), e.g., $E^{[2]}_{DD}(^2D_{3/2})^*$, represents the result at unit values of the relevant reduced matrix elements, and can be calculated from the results shown in Table III by dividing by the product of the matrix elements listed there.

The remaining step before the observed energies can be fit to extract core properties is to describe the small corrections that need to be applied prior to the fit. The goal is to calculate and subtract from the measured positions any contributions that would not be represented by Eq. (5). The simplest of these, and the only correction that was applied in the case of the optical RESIS study, is the relativistic correction to the Rydberg electron's energy,

$$
E_{\text{rel}}(q,n,L) = \frac{\alpha_{FS}^2 q^4}{2n^4} \left(\frac{3}{4} - \frac{n}{L+\frac{1}{2}} \right). \quad (6)
$$

This is evaluated for each level of this study and shown in column 2 of Table IV.

Another standard correction represents the energy shifts of the states under study due to their coupling to other Rydberg levels, i.e., other levels where the core ion remains in its ground electronic state. The lowest multipole term contributing to these shifts is due to the quadrupole moment of the core, but additional terms can be represented by the effects of V_{eff} in second order.

$$
E^{[2]}(V_{\text{eff}}) \equiv - \sum_{\substack{n',L' \\ J=\frac{5}{2},\frac{7}{2}}} \frac{\langle ^2F_{5/2},nL_K|V_{\text{eff}}|^2F_J,n'L'_K\rangle^2}{\Delta E(J'_C) + E(n') - E(n)}. \quad (7)
$$

Evaluating these energy shifts requires knowledge of the coefficients occurring in V_{eff}, but these shifts are usually quite small so an iterative approach is practical. The core properties appearing in V_{eff} are first extracted from the data ignoring Eq. (7), then used to calculate the corrections of Eq. (7), correct the data, and repeat the extraction of core properties. After a few iterations, stable results are found. As long as V_{eff} represents the fine-structure pattern, with only minor nonadiabatic effects, evaluation of Eq. (7) is straightforward. However, in the present case the large nonadiabatic effects of the $6d$ levels complicate the situation. In particular, two of the most significant terms in Eq. (7) are

TABLE V. Application of the corrections, from Table IV, to the measured energy levels, from Table II, to form the corrected energy levels that will be fit to determine core properties. All results are in MHz. Note that the net uncertainty in the corrected level positions is dominated by the uncertainty in the correction for $L = 9,10$, and by the measurement uncertainty for $L = 11,12$.

(L,K)	E_{obs}	$E_{\text{Corrections}}$	$E_{\text{corrected}}$
(9,6.5)	−5661.28(13)	16.64(8.21)	−5677.92(8.21)
(9,7.5)	−6514.38(16)	−64.75(5.92)	−6449.63(5.92)
(9,8.5)	−6736.10(31)	−57.54(4.28)	−6678.56(4.92)
(9,9.5)	−6232.58(39)	−181.58(20.90)	−6051.00(20.90)
(9,10.5)	−4363.80(32)	−58.91(3.08)	−4304.89(3.10)
(9,11.5)	—	−51.97(3.48)	—
(10,7.5)	−2168.86(7)	−32.81(1.24)	−2136.05(1.25)
(10,8.5)	−3387.82(16)	−44.48(0.83)	−3343.34(0.84)
(10,9.5)	−4053.08(26)	−40.20(0.74)	−4012.88(0.78)
(10,10.5)	−3975.28(30)	−55.43(1.04)	−3919.85(1.08)
(10,11.5)	−2862.11(33)	−47.11(0.57)	−2815.00(0.66)
(10,12.5)	—	−44.66(0.69)	—
(11,8.5)	−405.22(11)	−38.25(0.06)	−366.97(0.12)
(11,9.5)	−1724.35(18)	−37.51(0.03)	−1686.84(0.18)
(11,10.5)	−2548.18(28)	−35.73(0.05)	−2512.45(0.29)
(11,11.5)	−2705.10(33)	−42.00(0.19)	−2663.10(0.38)
(11,12.5)	−1977.51(33)	−40.78(0.19)	−1936.73(0.38)
(11,13.5)	—	−39.31(0.06)	—
(12,9.5)	0.00(28)	−34.07(0.01)	34.07(0.28)
(12,10.5)	−1125.67(19)	−33.43(0.00)	−1092.24(0.19)
(12,11.5)	−1831.35(29)	−32.26(0.02)	−1799.09(0.29)
(12,12.5)	−1985.76(30)	−35.56(0.08)	−1950.20(0.31)
(12,13.5)	−1428.20(34)	−35.67(0.22)	−1392.53(0.41)
(12,14.5)	—	−34.66(0.02)	—

the terms proportional to $(\alpha_{D,0})^2$ and $Q\alpha_{D,0}$. Since, as will be shown below, about 40% of the scalar dipole polarizability, $\alpha_{D,0}$, is due to coupling to the $6d$ levels, the straightforward evaluation of Eq. (7) is probably not correct for these large terms. The terms in question actually represent portions of the fourth-order and third-order perturbation energies, simplified by the adiabatic expansion of the energy denominators that occur. The portion of the shifts due to the $6d$ levels can be evaluated without this approximation, giving slightly different results [10]. The other terms are small enough that the adiabatic expressions are probably adequate. Column 3 of Table IV shows the total calculated correction due to Eq. (7), with an uncertainty assigned due to the complications involving the $6d$ levels.

Another significant correction results from coupling between different $n = 28$ Rydberg levels bound to the core ground state and sharing the same K. An example would be the energy shift of the (9,9.5) level due to coupling to the (7,9.5) level. Fortunately, the quadrupole coupling between these levels, and other similar level pairs is zero due to the selection rule on hydrogenic radial functions,

$$[nL|r^{-3}|nL \pm 2] = 0. \qquad (8)$$

Consequently, the lowest-order coupling is due to $\alpha_{D,2}$, the tensor dipole polarizability. The energy shift due to this coupling is not described by Eq. (7) since the denominator

of Eq. (7) is zero for cases of this type. Clearly, however, these levels are not degenerate since they have different fine-structure energies. Once the $n = 28$ energy level pattern is understood, these shifts can be evaluated. Once again, the nonadiabatic response of the $6d$ levels complicates the situation. In fact, as will be shown below, almost all of $\alpha_{D,2}$ is due to the $6d$ levels. Consequently, the couplings responsible for these energy shifts need to be evaluated without making the adiabatic approximation [10]. The uncertainties in the resulting energy shifts, especially for the $L = 9$ and $L = 10$ levels, are dominated by uncertainties in the positions of the perturbing levels. The calculated shifts are shown in column 4 in Table IV.

The last correction shown in Table IV is necessary because of the very large size of the second-order dipole-dipole energies due to the $6d\,^2D_{3/2}$ core level, column 2 in Table III. These shifts are calculated from Eq. (3) above, and they represent energy shifts in the $n = 28$ level under study from coupling to members of the Rydberg series bound to the $^2D_{3/2}$ core level. Some of these energy shifts are so large that the approximation implicit in Eq. (3)—that the energy of the perturbing level is given by its zeroth-order energy—is not adequate. Specifically, this is a problem for the perturbing levels closest to $n = 28$. For example, the zeroth-order energy of the $n' = 10$ level bound to the $^2D_{3/2}$ ($\Delta E = 9193.2462$ cm^{-1}) is only 576.62 cm^{-1} above the $n = 28$ level, and this level alone shifts the $n = 28$ (9,6.5) level by about -5000 MHz. The fine-structure energies in the $n' = 10$ level are estimated to be on the order of 10 cm^{-1}, so neglecting these mis-states the energy difference of the perturbing levels by 1%–2%, and changes the calculated energy shift of the $n = 28$ level by 50–100 MHz. To account for this, it is necessary to simulate the fine-structure energies of the $^2D_{3/2}$ Rydberg levels closest to $n = 28$, specifically $n' = 9$, 10, and 11. This, in turn, requires estimates of the quadrupole moment and polarizabilities of the $^2D_{3/2}$ core state. Fortunately, theoretical estimates of these properties have been reported. The quadrupole moment has been estimated to be 1.32 a.u. [13], and the adiabatic scalar and tensor dipole polarizabilities have been calculated to be $(\alpha_{D,0}, \alpha_{D,2}) = [4.5(8), -1.6(2)]$ [11]. Here again, the nonadiabatic coupling between the $6d\,^2D_{3/2}$ state and the ground state complicates the situation. This coupling alone is calculated to contribute $-9.3(8)$ a.u. to the total scalar polarizability, but judging from the analogous effects in the $n = 28$ Rydberg levels, this could be a substantial underestimate of its influence on the Rydberg energies. To correct for this, we will multiply this contribution by a factor of 2.0(5), and reach a revised estimate of $\alpha_{D,0} = -4.5(4.5)$ a.u. Using these properties of the $6d\,^2D_{3/2}$ state, the deviations from hydrogenic energies for the most nearly degenerate intermediate levels bound to this state were calculated, and the resulting changes in the second-order dipole-dipole energies due to the $^2D_{3/2}$ series were evaluated. These corrections are shown in column 5 of Table IV.

The sum of the four calculated corrections is shown in the last column of Table IV. Table V applies these corrections by subtracting them from the experimentally determined level energies, from Table II. For the $n = 28$ $L = 9$ and $L = 10$ levels, the uncertainties in the corrections are larger than the experimental errors, and will limit the precision of the analysis.

TABLE VI. Decomposition of the largest terms of $\langle V_{\text{eff}}^{\text{Mod}} \rangle$ at the fitted parameter values. The first column identifies the $n = 28$ level. The next six columns show the contributions proportional to the parameter listed at the top of the column. The eighth column shows the total contribution from all other parameters, and the last column shows the total. All results are in MHz.

(L,K)	A_0	A_{04}	A_{23}	A_{24}	A_{45}	A_{13}	Other	$\langle V_{\text{eff}}^{\text{Mod}} \rangle$
(9,6.5)	−157.5	−2181.3	3302.2	−16.3	11.2	7.8	−30.0	936.1
(9,7.5)	−157.5	−2181.3	330.2	−1.6	−22.5	5.5	−18.2	−2045.5
(9,8.5)	−157.5	−2181.3	−1754.9	8.7	4.8	2.8	−31.7	−4109.1
(9,9.5)	−157.5	−2181.3	−2471.9	12.2	18.7	−0.2	−36.8	−4816.7
(9,10.5)	−157.5	−2181.3	−1283.1	6.3	−16.0	−3.4	−19.5	−3654.5
(9,11.5)	−157.5	−2181.3	2405.9	−11.9	3.9	−7.1	−32.7	19.4
(10,7.5)	−157.5	−1307.4	2405.9	−9.6	5.2	6.4	−11.3	931.5
(10,8.5)	−157.5	−1307.4	175.0	−0.7	−10.8	4.4	−7.4	−1304.5
(10,9.5)	−157.5	−1307.4	−1342.7	5.4	2.8	2.2	−12.8	−2810.1
(10,10.5)	−157.5	−1307.4	−1822.0	7.3	8.8	−0.2	−14.2	−3285.3
(10,11.5)	−157.5	−1307.4	−903.4	3.6	−7.9	−2.9	−7.3	−2382.9
(10,12.5)	−157.5	−1307.4	1806.8	−7.2	2.0	−5.8	−13.0	317.7
(11,8.5)	−157.5	−819.9	1806.8	−6.0	2.6	5.3	−4.6	826.6
(11,9.5)	−157.5	−819.9	90.3	−0.3	−5.5	3.6	−3.3	−892.6
(11,10.5)	−157.5	−819.9	−1047.9	3.5	1.6	1.8	−5.6	−2024.1
(11,11.5)	−157.5	−819.9	−1380.4	4.6	4.5	−0.3	−6.0	−2355.0
(11,12.5)	−157.5	−819.9	−657.7	2.2	−4.2	−2.5	−2.9	−1642.5
(11,13.5)	−157.5	−819.9	1391.2	−4.6	1.1	−4.9	−5.7	399.7
(12,9.5)	−157.5	−533.8	1391.2	−3.8	1.3	4.5	−2.0	699.9
(12,10.5)	−157.5	−533.8	42.8	−0.1	−3.0	3.0	−1.6	−650.1
(12,11.5)	−157.5	−533.8	−832.4	2.3	1.0	1.4	−2.6	−1521.6
(12,12.5)	−157.5	−533.8	−1070.2	3.0	2.4	−0.3	−2.7	−1759.1
(12,13.5)	−157.5	−533.8	−492.3	1.4	−2.3	−2.1	−1.2	−1187.9
(12,14.5)	−157.5	−533.8	1094.0	−3.0	0.6	−4.1	−2.6	393.5

For the $L = 11$ and $L = 12$ levels, this is not the case. These corrected energies were fit to Eq. (5), with

$$\langle V_{\text{eff}}^{\text{Mod}} \rangle = A_0 + [A_{04}\langle r^{-4}\rangle + A_{06}\langle r^{-6}\rangle] + [A_{13}\langle r^{-6}\rangle + A_{16}\langle r^{-6}\rangle]\vec{L} \cdot \vec{J}_c + [A_{23}\langle r^{-3}\rangle + A_{24}\langle r^{-4}\rangle] \frac{X^{[2]}(J_c) \cdot C^{[2]}(\hat{r})}{\begin{pmatrix} J_c & 2 & J_c \\ -J_c & 0 & J_c \end{pmatrix}}$$

$$+ [A_{35}\langle r^{-5}\rangle]X^{[3]}(J_c) \cdot T^{[3]}(\hat{r}) + [A_{45}\langle r^{-5}\rangle + A_{46}\langle r^{-6}\rangle] \frac{X^{[4]}(J_c) \cdot C^{[4]}(\hat{r})}{\begin{pmatrix} J_c & 4 & J_c \\ -J_c & 0 & J_c \end{pmatrix}}. \tag{9}$$

The constant term, A_0, corrects for the arbitrary assignment of the energy of the (12,9.5) level as zero. The other nine coefficients represent the terms shown in Eq. (2), except that the r^{-8} term in the third-order tensor term has been omitted. Of course, none of the core properties represented by these coefficients include contributions from the $6d$ levels. The ten parameters in Eq. (9) plus the two matrix elements from Eq. (5) make a 12-parameter fit of the 20 corrected level positions from Table V. The fit returns the following parameters:

$$A_0 = -157.5(1.5),$$

$$A_{04} = -4.753(16), \quad A_{06} = -19.0(7.3),$$

$$A_{13} = -3.31(98) \times 10^{-5}, \quad A_{16} = -0.04(44),$$

$$A_{23} = -0.5931(14), \quad A_{24} = 0.061(55),$$

$$A_{35} = 0.11(25),$$

$$A_{45} = 0.69(28), \quad A_{46} = -5.4(7.7),$$

$$\langle ^2F_{5/2}||M^{[1]}||\,^2D_{3/2}\rangle = -1.436(2), \quad \langle ^2F_{5/2}||M^{[3]}||\,^2D_{3/2}\rangle = 3.3(1.1).$$

The fit determines the relative sign of the two matrix elements, but is insensitive to the absolute sign. The fit is satisfactory. The chi squared is 13 for eight degrees of freedom. All but two of the levels are fit to within their uncertainty. Because the

TABLE VII. Summary of the fit of measured $n = 28$ fine structure in Th^{2+}. The first column identifies the level. Column 2 shows the expectation value of $V_{\text{eff}}^{\text{Mod}}$, from Table VI. The next two columns show the total dipole-dipole and octupole-dipole second-order perturbation energies from intermediate states containing $6d$ levels of the core ion. Column 5 shows the total correction from Table IV. The total fitted energy is shown in column 6, with the uncertainty from the quadrature sum of experimental and correction uncertainty. Column 7 shows the measured energy, from Table II, and column 8 shows the difference between the measured and fitted energies. All results are in MHz.

(L,K)	$\langle V_{\text{eff}}^{\text{Mod}} \rangle$	$E^{[2]}(^2D_{3/2})$ and $E^{[2]}(^2D_{5/2})$	$E_{OD}^{[2]}(^2D_{3/2})$ and $E_{OD}^{[2]}(^2D_{5/2})$	$E_{\text{Corrections}}$	$E_{\text{Predicted}}$	E_{obs}	$E_{\text{obs}} - E_{\text{Predicted}}$
(9,6.5)	936.1	−6564.7	−26.6	16.6	−5638.6(8.2)	−5661.28(13)	−22.7
(9,7.5)	−2045.5	−4426.9	24.9	−64.8	−6512.3(5.9)	−6514.38(16)	−2.1
(9,8.5)	−4109.1	−2581.2	9.9	−57.5	−6737.8(4.3)	−6736.10(31)	1.7
(9,9.5)	−4816.7	−1243.8	−10.5	−181.6	−6252.6(20.9)	−6232.58(39)	20.1
(9,10.5)	−3654.5	−656.7	3.1	−58.9	−4367.1(3.1)	−4363.80(32)	3.3
(9,11.5)	19.4	−1087.2	−2.6	−52.0	−1122.3(3.5)	—	—
(10,7.5)	931.5	−3060.6	−8.5	−32.8	−2170.4(1.2)	−2168.86(7)	1.5
(10,8.5)	−1304.5	−2047.2	8.2	−44.5	−3388.0(0.8)	−3387.82(16)	0.1
(10,9.5)	−2810.1	−1205.2	2.9	−40.2	−4052.7(0.7)	−4053.08(26)	−0.4
(10,10.5)	−3285.3	−631.5	−3.4	−55.4	−3975.7(1.0)	−3975.28(30)	0.4
(10,11.5)	−2382.9	−433.2	1.5	−47.1	−2861.6(0.6)	−2862.11(33)	−0.5
(10,12.5)	317.7	−727.5	−1.2	−44.7	−455.6(0.7)	—	—
(11,8.5)	826.6	−1191.4	−2.1	−38.3	−405.2(0.1)	−405.22(11)	0.0
(11,9.5)	−892.6	−796.4	2.0	−37.5	−1724.4(0.0)	−1724.35(18)	0.1
(11,10.5)	−2024.1	−488.8	0.6	−35.7	−2548.1(0.1)	−2548.18(28)	−0.1
(11,11.5)	−2355.0	−307.5	−0.8	−42.0	−2705.3(0.2)	−2705.10(33)	0.2
(11,12.5)	−1642.5	−294.9	0.7	−40.8	−1977.4(0.2)	−1977.51(33)	−0.1
(11,13.5)	399.7	−497.0	−0.6	−39.3	−137.2(0.1)	—	—
(12,9.5)	699.9	−665.0	−0.8	−34.1	0.0(0.01)	0.00(28)	0.0
(12,10.5)	−650.1	−442.9	0.8	−33.4	−1125.7(0.0)	−1125.67(19)	0.0
(12,11.5)	−1521.6	−277.7	0.2	−32.3	−1831.4(0.0)	−1831.35(29)	0.0
(12,12.5)	−1759.1	−190.8	−0.3	−35.6	−1985.7(0.1)	−1985.76(30)	0.0
(12,13.5)	−1187.9	−205.2	0.4	−35.7	−1428.4(2)	−1428.20(34)	0.2
(12,14.5)	393.5	−346.0	−0.3	−34.7	12.5(0.0)	—	—

reduced chi squared is slightly greater than 1, the parameter errors have been increased to reflect this. Tables VI and VII detail the results of the fit. Table VI breaks down the largest contributions to $\langle V_{\text{eff}} \rangle$, and Table VII shows the complete predictions of the fit and the residuals. The fit is particularly good for the $L = 11$ and $L = 12$ levels, where the residuals are smaller than the measurement errors.

One conclusion that can be drawn from the fitted parameters is that the actual energy of the (12,9.5) level, which was arbitrarily assigned a value of zero in Table II, is 157.5(1.5) MHz above the nonrelativistic hydrogenic energy of an $n = 28$ Rydberg level. Two fitted parameters give information about permanent electric moments of the Th^{3+} ground state. The quadrupole moment is related to the parameter A_{23}.

$$Q = -A_{23} = 0.5931(14) \text{ a.u.},$$

and the hexadecapole moment is related to the fitted parameter A_{45}.

$$\Pi = -A_{45} = -0.69(28) \text{ a.u.}$$

The magnetic dipole moment, or g factor, is related to the fitted parameter A_{13}.

$$g_J = -\frac{2}{\alpha_{FS}^2} A_{13} = 1.24(48).$$

This is completely consistent with the Landé g factor for a $^2F_{5/2}$ level, 6/7. The fitted value of A_{35} is consistent with zero, indicating no significant contribution from a permanent magnetic octupole moment.

The other fitted parameters are related to polarizabilities of Th^{3+}. The parameter A_{04} is related to the scalar dipole polarizability.

$$\alpha_{D,0}^{\text{Mod}} = -2A_{04} = 9.51(3) \text{ a.u.}$$

The parameter A_{06} is related to the scalar quadrupole polarizability.

$$\alpha_{Q,0} = -2A_{06} + 6\beta_{D,0}^{\text{Mod}},$$

where $\beta_{D,0}^{\text{Mod}}$ is the first nonadiabatic scalar dipole polarizability excluding contributions from the $6d$ levels. The quadrupole polarizability would be the total quadrupole polarizability since the $6d$ levels do not contribute. In order to extract a value of $\alpha_{Q,0}$ it is necessary to have an estimate of $\beta_{D,0}^{\text{Mod}}$. $\beta_{D,0}^{\text{Mod}}$ is closely related to $\alpha_{D,0}^{\text{Mod}}$, and depends on the same set of matrix elements and excitation energies [1]. The majority of the $\alpha_{D,0}^{\text{Mod}}$(7.70 a.u.) is due to the excitation of the core Th^{4+} ion [9,14], and the contributions to $\beta_{D,0}^{\text{Mod}}$ from these excitations

TABLE VIII. The measured and calculated properties of Th^{3+} Column 1 gives the properties. The second column gives the results extracted from the rf measurements of the $n = 28$ Th^{2+} Rydberg fine structure. Column 3 gives the result from the optical RESIS study of the Th^{2+} Rydberg fine structure. The final column gives the recent theoretical results for the properties. The units on all the properties in the table are atomic units.

Property	This work (a.u.)	Optical[a] (a.u.)	Theory (a.u.)
$\alpha_{D,0}$	15.224(33)	15.42(17)	14.67(60)[b]
$\alpha_{D,0}^{\text{Mod}}$	9.51(3)	9.67(15)	8.81(34)[b]
Q	0.5931(14)	0.54(4)	0.624(14)[b]
$\alpha_{D,2}^{\text{Mod}}$	$-0.12(11)$	1.5(1.3)	$-0.19(13)$[b]
$\alpha_{D,2}$	$-5.30(11)$	$-3.6(1.3)$	$-6.07(53)$[b]
$\alpha_{Q,0}$	60(15)	—	—
Π	$-0.69(28)$	—	-0.76[c]
$\|\langle 5^2 F_{5/2}\|M^{[1]}\|6^2 D_{3/2}\rangle\|$	1.436(2)	1.435(10)	1.530(63)[b]
$\|\langle 5^2 F_{5/2}\|M^{[3]}\|6^2 D_{3/2}\rangle\|$	3.3(1.1)	—	8.394[c]

[a]Reference [2].
[b]Reference [11].
[c]Private communication with Safronova [12].

have been calculated as [14]

$$\left(\beta_{D,0}^{\text{Mod}}\right)_{\text{core}} = 2.97(15) \text{ a.u.}$$

The remainder of the $\alpha_{D,0}^{\text{Mod}}$, 1.81 a.u. is due to valence excitations of Th^{3+} to states other than the $6d$ levels. Since all of these levels have excitation energies >0.7 a.u. [11], an upper limit of their contribution is

$$\left(\beta_{D,0}^{\text{Mod}}\right)_{\text{valence}} \leqslant \left(\frac{\alpha_{D,0}^{\text{Mod}}}{2\Delta E}\right) = 1.2 \text{ a.u.}$$

Taking $(\beta_{D,0}^{\text{Mod}})_{\text{valence}} \sim 0.6(6)$ a.u., we find $\beta_{D,0}^{\text{Mod}} = 3.6(6)$ a.u. Using that result it is possible to extract a value for the scalar quadrupole polarizability from the result of the fit of the data.

$$\alpha_{Q,0} = 38(15) + 22(4) = 60(15) \text{ a.u.}$$

The tensor dipole polarizability is related to the fitted parameter A_{24}.

$$\alpha_{D,2}^{\text{Mod}} = -2A_{24} = -0.12(11) \text{ a.u.}$$

The small value of $\alpha_{D,2}^{\text{Mod}}$ indicates that virtually all of the tensor polarizability is due to the $6d$ levels.

Two other significant results from the fits are determinations of the dipole and octupole reduced matrix elements coupling the ground state to the $6d\ ^2D_{3/2}$ level.

$$\|\langle ^2F_{5/2}\|M^{[1]}\|^2D_{3/2}\rangle\| = 1.436(2),$$
$$\|\langle ^2F_{5/2}\|M^{[3]}\|^2D_{3/2}\rangle\| = 3.3(1.1).$$

The dipole matrix elements can be used to calculate the contribution of the $6d$ levels to the total scalar and tensor dipole polarizabilities, since these are simply related to the

coupling matrix elements [1].

$$\alpha_{D,0} = \alpha_{D,0}^{\text{Mod}} + \alpha_{D,0}(^2D_{3/2}) + \alpha_{D,0}(^2D_{5/2})$$
$$= 9.51(3) + 5.466(14) + 0.248(1) = 15.224(33) \text{ a.u.}$$

$$\alpha_{D,2} = \alpha_{D,2}^{\text{Mod}} + \alpha_{D,2}(^2D_{3/2}) + \alpha_{D,2}(^2D_{5/2})$$
$$= -0.12(11) - 5.466(14) + 0.283(1) = -5.30(11) \text{ a.u.}$$

While these adiabatic polarizabilities do not directly describe the $n = 28$ Rydberg levels studied here, they would apply in other applications such as the interaction with static electric fields.

IV. DISCUSSION

Table VIII summarizes the Th^{3+} properties determined from this study. Column 1 identifies the property, and column 2 shows the value obtained here. Column 3 shows the values inferred from the optical RESIS study, for comparison. The results of this study are on average an order of magnitude more precise than the optical study, and this study also reports more properties. The present results are in good agreement with the less precise results inferred from the optical study, despite the sparse data pattern available in the optical study. The final column in Table VIII gives the most recent theoretical predictions for the Th^{3+} properties reported here [11,12]. This recent theoretical study includes consideration of the various levels of theory that could be applied to this problem, ranging from a single configuration Dirac-Fock calculation to a sophisticated relativistic many body perturbation theory approach. It is interesting to note that the predictions obtained in the several approaches considered often varied by up to a factor of 2 [11]. In most cases, this theoretical study also assigned uncertainties to the theoretical predictions, based on the size of correlation corrections encountered, and these uncertainties are about an order of magnitude larger than the experimental uncertainties reported here. In general, the agreement between theory and experiment is within several standard deviations. The excellent agreement for the total adiabatic scalar dipole polarizability, $\alpha_{D,0}$, is apparently fortuitous, since neither $\alpha_{D,0}^{\text{Mod}}$ or the portion of $\alpha_{D,0}$ due to the $6d$ levels agrees with the calculation. The measured hexadecapole moment agrees with the only available calculation. In contrast, the measured octupole matrix element connecting the ground state to the $6d\ ^2D_{3/2}$ level differs from theory by a factor of more than 2. We are unaware of any theoretical predictions for the scalar quadrupole polarizability. Overall, the Th^{3+} properties reported provide insight into the behavior of a highly relativistic f-electron ion and a benchmark test of very challenging atomic structure calculations.

[1] S. L. Woods and S. R. Lundeen, Phys. Rev. A **85**, 042505 (2012).

[2] J. A. Keele, M. E. Hanni, S. L. Woods, S. R. Lundeen, and C. W. Fehrenbach, Phys. Rev. A **83**, 062501 (2011).

[3] J. Blaise and J. F. Wyart, http://www.lac.u-psud.fr/Database/Contents.html.

[4] C. J. Campbell, A. V. Steele, L. R. Churchill, M. V. DePalatis, D. E. Naylor, D. N. Matsukevich, A. Kuzmich, and M. S. Chapman, Phys. Rev. Lett. **102**, 233004 (2009).

[5] U. I. Safronova, W. R. Johnson, and M. S. Safronova, Phys. Rev. A **76**, 042504 (2007).

[6] V. Goncharov and M. C. Heaven, J. Chem. Phys. **124**, 064312 (2006).

[7] E. Peik and C. Tamm, Europhys. Lett. **61**, 181 (2003).

[8] S. Woods, C. Smith, J. Keele, and S. R. Lundeen, Phys. Rev. A **87**, 022511 (2013).

[9] J. A. Keele, C. S. Smith, S. R. Lundeen, and C. W. Fehrenbach, Phys. Rev. A **85**, 064502 (2012).

[10] Julie A. Keele, Ph.D thesis, Colorado State University, 2013.

[11] M. S. Safronova and U. I. Safronova, Phys. Rev. A **87**, 062509 (2013).

[12] M. S. Safronova (private communication).

[13] U. I. Safronova (private communication).

[14] U. I. Safronova and M. S. Safronova, Phys. Rev. A **84**, 052515 (2011).